Real-time monitoring of hydrogel phase transition in an ultrahigh *Q* microbubble resonator

Daquan Yang,[1] Aiqiang Wang,[1] Jin-Hui Chen,[2] Xiao-Chong Yu,[2] Chuwen Lan,[1] Yuefeng Ji,[1] and Yun-Feng Xiao[2,3,4,5,*]

[1]State Key Laboratory of Information Photonics and Optical Communications, School of Information and Communication Engineering, Beijing University of Posts and Telecommunications, Beijing 100876, China
[2]State Key Laboratory for Artificial Microstructure and Mesoscopic Physics, School of Physics, Peking University, Beijing 100871, China
[3]Frontiers Science Center for Nano-optoelectronics & Collaborative Innovation Center of Quantum Matter, Beijing 100871, China
[4]Collaborative Innovation Center of Extreme Optics, Shanxi University, Taiyuan 030006, China
[5]Beijing Academy of Quantum Information Sciences, Beijing 100193, China
*Corresponding author: yfxiao@pku.edu.cn

The ability to sense dynamic biochemical reactions and material processes is particularly crucial for a wide range of applications, such as early-stage disease diagnosis and biomedicine development. Optical microcavities-based label-free biosensors are renowned for ultrahigh sensitivities, and the detection limit has reached a single nanoparticle/molecule level. In particular, a microbubble resonator combined with an ultrahigh quality factor (*Q*) and inherent microfluidic channel is an intriguing platform for optical biosensing in an aqueous environment. In this work, an ultrahigh *Q* microbubble resonator-based sensor is used to characterize dynamic phase transition of a thermosensitive hydrogel. Experimentally, by monitoring resonance wavelength shift and linewidth broadening, we (for the first time to our knowledge) reveal that the refractive index is increased and light scattering is enhanced simultaneously during the hydrogel hydrophobic transition process. The platform demonstrated here paves the way to microfluidical biochemical dynamic detection and can be further adapted to investigating single-molecule kinetics.   © 2020 Chinese Laser Press

https://doi.org/10.1364/PRJ.380238

1. INTRODUCTION

Monitoring and controlling the phase transition dynamics of materials is very important for both fundamental studies and practical applications [1–3], e.g., transformation of matter state, ferromagnetic phase transition, superconductor dynamics, and hydrogel phase transition dynamics. As a crucial phase-transition material, hydrogels are a class of biomaterials with a broad range of applications, such as in biochemistry and biopharmaceutics [4–7]. To monitor the hydrogel phase-transition process, several methods have been developed, including nuclear magnetic resonance (NMR) and rheology. However, the NMR method is with high cost, requires specialized equipment, and is hampered by low resolution in aqueous environments [8]. As for the rheology method, it cannot be easily implemented to study rapid gelling dynamics or mechanically weak materials [9]. On the other hand, optical microcavities of ultrahigh quality factors (*Q*) and small volumes [10] can significantly enhance light–matter interactions. Therein, whispering gallery mode (WGM) microresonator-based label-free biosensors are renowned for their ultrahigh sensitivities and

low detection limit [11–19]. In particular, several WGM microresonator systems have achieved single nanoparticles [20–33], molecules (e.g., viruses, proteins, and DNAs) [34–46], and even atomic ions [47]. However, there have been few demonstrations yet that these systems can be used to investigate the dynamics of biochemical reactions [48].

Herein, real-time monitoring of the hydrogel phase transition (i.e., hydrophilic transition and hydrophobic transition) in WGM microbubble resonator (MBR)-based sensors is first demonstrated by continuously monitoring both wavelength shift and linewidth broadening simultaneously. Experimentally, the thermosensitive hydrogel phase transition is optically controlled by increasing/decreasing the irradiation light power (∼1550 nm). During a hydrophilic to hydrophobic transition process, an overall wavelength redshift ∼40 pm and a distinct linewidth broadening over 10 times are observed, respectively. The WGM linewidth broadening unambiguously reveals the hydrogel phase transition due to the enhanced light scattering, and the refractive index changes are detected by monitoring wavelength shift. Note that compared with the wavelength shift

sensing mechanism, the WGM linewidth broadening is immune to noises, including thermal noise and laser frequency noise in practical measurements. The results shown in this work demonstrate that optical MBR is a promising platform for further investigating the biochemical dynamics and molecule kinetics [44].

2. MBR FABRICATION AND CHARACTERIZATION

The experimental measurement setup is shown in Fig. 1(a). The MBR is chosen to investigate and characterize the phase transition of poly(N-isopropylacrylamide)-based hydrogel (PNIPA), owing to its high Q factor, easy fabrication, and intrinsic microfluidic characteristics. The PNIPA hydrogel fabrication recipe is based on Ref. [49]. To fabricate the MBR, the capillary with a tapered waist diameter of 30 μm (outer diameter) is first drawn from a silica capillary (TSP-100170, outer diameter of 140 μm, inner diameter of 100 μm, and $n = 1.45$) using a hydrogen flame. Then, the tapered silica capillary is pressurized with three atmospheric pressures of the air. The MBR (wall thickness is 1–2 μm) is formed by heating an internally pressurized silica capillary using two counterpropagating focused CO_2 laser beams, where the wall in the heated region expands and becomes thinner [30]. The typical MBR size used in the experiment is ~80 μm in diameter. Here, the temperature-responsive PNIPA hydrogel is employed for its critical temperature (~32°C) lying in the desired range of 25–35°C [49–52]. The PNIPA hydrogel is synthesized by the *in situ* polymerization of the monomer in deionized water (DI water) [49], and is filled into the MBR. The thermosensitive phase transition in PNIPA is optically controlled by adjusting the power of the irradiation light from a single-mode fiber (SMF), as shown in Fig. 1(a). The control light is chosen at infrared band (~1550 nm), considering the significant

light absorption of water, leading to effective control of the temperature changes in the PNIPA solution.

As shown in Fig. 1(a), a tunable laser (Newport, TLB-6712) at 780-nm wavelength band is used to efficiently excite the WGMs of the MBR via fiber–taper coupling. A fiber polarization controller is adjusted manually to control the polarization of the input laser and achieve the maximum light coupling efficiency. The transmission light signal is collected and detected in real time by a low-noise photodetector (New Focus, 1801-FC) and analyzed by an oscilloscope. To demonstrate the ultrahigh Q factor of the WGMs of the MBR, the MBR is coupled with the optical microfiber through the evanescent field, and there is no contact between the MBR and fiber. A representative transmission spectrum of a typical MBR filled with the PNIPA solution is shown in Fig. 1(c). Although the absorption of the PNIPA solution to the probe light can spoil the Q factors of the microbubble cavity, the corresponding mode still possesses an ultrahigh Q factor of 9.11×10^7, as shown in Fig. 1(d). This is mainly due to the relatively small field distribution of WGMs inside the PNIPA solution, as shown in Fig. 1(e). Remarkably, as depicted in Fig. 1(b), the reaction dynamics (i.e., phase transition including hydrophilic transition and hydrophobic transition) of the PNIPA is monitored continuously by real-time tracking of the wavelength shift and linewidth broadening when the control power of the irradiation light changes. As the control power increases, the WGMs exhibit redshift and linewidth broadening during the hydrophobic transition process. Conversely, as the control power decreases, the WGMs exhibit blueshift and linewidth narrowing during the hydrophilic transition process.

3. MBR FOR MONITORING HYDROGEL PHASE TRANSITION

To make the measurement more reliable and stable, the fiber–taper is attached to the surface of the MBR during the
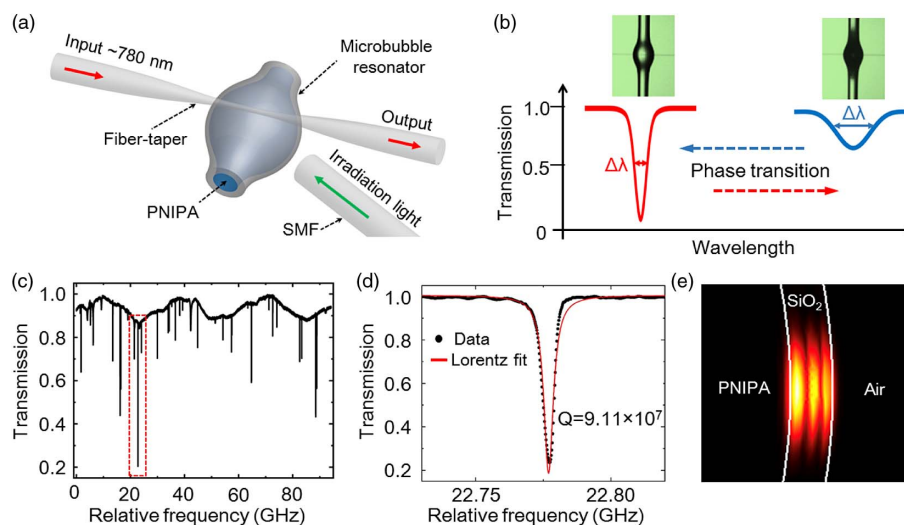

Fig. 1.   (a) Schematic of the MBR platform for real-time monitoring of the dynamic reactions of hydrogel phase transition. The thermosensitive phase transition of PNIPA is optically controlled by the irradiation light power (~1550 nm) from an SMF. (b) Monitoring the phase transition dynamics of the PNIPA solution by tracking the wavelength shift and linewidth broadening of a WGM. Insets, CCD images of the microbubble with the PNIPA solution at hydrophilic and hydrophobic state, respectively. (c) Transmission spectrum of MBR with the PNIPA solution at hydrophilic state. The enlarged view of the red square region is shown in (d). (e) Typical optical field distribution of a WGM in the MBR by finite-element method simulation.

experiment. The infrared light (~1550 nm) is chosen as a stable local heating source (power fluctuation ±0.01 dB) to fine-tune the temperature of the MBR due to the balance between the light absorption and heat dissipation. As a result, the irradiation light power is equivalent to locally changing the temperature of PNIPA, and this laser heating method is extremely suitable for the study of hydrogel phase transition inside the MBR. Figures 2(a) and 2(b) show the evolution of transmission spectra of an MBR filled with the PNIPA solution when the control power of the irradiation light gradually changes. When the control power of the irradiation light first increases from 0 to 3.00 mW, the WGM resonance appears redshifted as the PNIPA hydrogel undergoes a hydrophilic to hydrophobic transition, which contributes to the increase of refractive index [48]. Then, when the control light power decreases from 3.00 to 0 mW, the WGM resonance is blueshifted during the hydrophilic transition process of the PNIPA hydrogel. It is found that the resonance is not perfectly shifting back to the original position after a cycle of hydrophilic–hydrophobic–hydrophilic transition. This small hysteresis phenomenon in PNIPA phase transition has been sufficiently demonstrated in previous work [53,54]. The phase transition of PNIPA can be visually resolved from the optical microscope images of the MBR, i.e., bright state (hydrophilic) to dark state (hydrophobic), which is contributed to by the enhanced light scattering [49], as will be discussed in detail in the following section.

To correlate the optical power for heating to the actual temperature change occurring in the MBR, a calibration curve is made from the DI water-filled MBR. We confirmed that the wavelength shift at 3.00 mW is 69.78 pm [black line in Fig. 3(a)], corresponding to a temperature of ~33°C, which is higher than the transition temperature of ~32°C [49].

Figures 3(a) and 3(b) show the typical resonance wavelength shift and linewidth broadening, respectively, of MBR in PNIPA, DI water, and air, as the irradiation light increases power from 0 to 3.00 mW. We do the measurements after a period of time (over 30 s), such that the temperature reaches a stable condition at each laser power. We find that the wavelength shift and linewidth broadening of the WGM can directly reflect the phase-transition process of the PNIPA solution. The transmission spectra are fitted by Lorentzian line shapes from which the linewidth of a WGM can be obtained. This fitting procedure is improved by an iteration of weighted least-squared regression [22]. It is intuitive that for the MBR filled with air, minor wavelength shift and linewidth broadening are observed as the power of the irradiation light increases because of the weak absorption of silica. On the other hand, for the MBR filled with DI water and PNIPA hydrogel, its wavelength strongly redshifts because of the increasing power of the irradiation light. The water-core MBR shows an almost linear wavelength redshift and no obvious linewidth change, since the infrared irradiation light only heats the water. Note that a hydrophilic to hydrophobic transition process of PNIPA can be clarified as four stages. (i) Pure hydrophilic state (0–1.44 mW): the PNIPA solution absorbs the control light, and the WGM of the MBR is redshifted due to the thermal-optic effect of silica. (ii) Subtransition state (1.44–2.04 mW): the PNIPA starts to transform from hydrophilic to hydrophobic state and absorbs energy from the environment [55]. In this transition process, on the one hand, the wavelength shift slope on irradiation power is decreased. We anticipate that the wavelength shift can mainly be attributed to the change of physical properties of PNIPA (e.g., thermal-optic response, volume shrink) [56,57]. On the other hand, the linewidth is increased, which
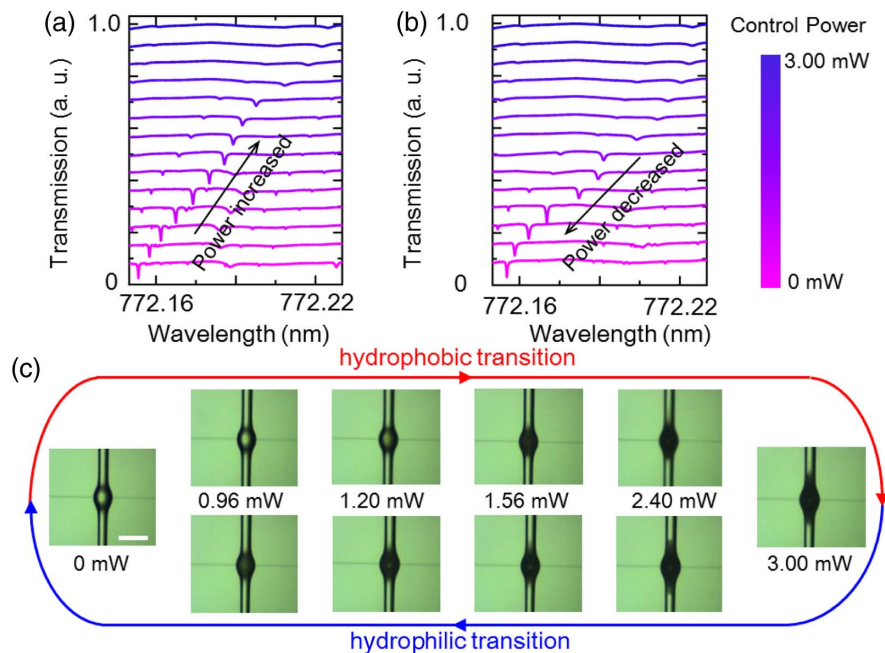

Fig. 2. Transmission evolution of the microbubble with the PNIPA hydrogel when the control power of the irradiation light first (a) increases from 0 to 3.00 mW, and then (b) decreases from 3.00 to 0 mW; (c) CCD images of a cycle of phase-transition process of the PNIPA hydrogel. The microbubble changes from transparent hydrophilic state to opaque hydrophobic state due to the increased scattering. Inset, the scale bar is 125 μm.
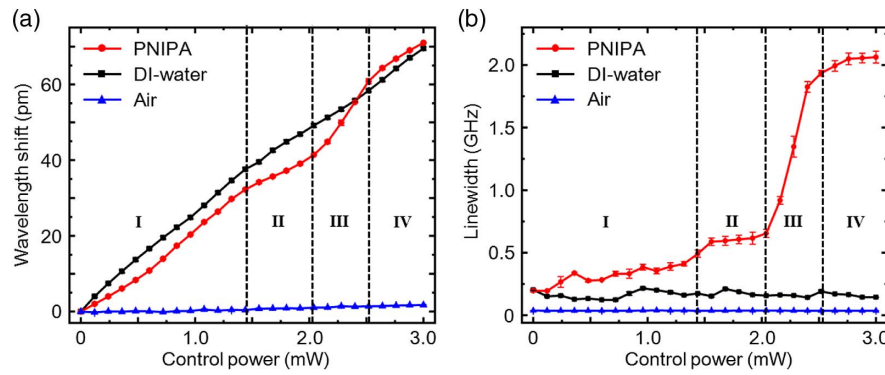
Fig. 3. (a) WGM wavelength shifts and (b) linewidth broadenings as a function of control power of the irradiation light from 0 to 3.00 mW, when the MBRs are filled with air (blue line with triangular marker), DI water (black line with square marker), and PNIPA hydrogel (red line with circular marker). Compared with the result of microbubble cavities filled with air and DI water, note that a hydrophilic to hydrophobic transition process of PNIPA can be clarified as four stages: (i) pure hydrophilic state (0–1.44 mW); (ii) subtransition state (1.44–2.04 mW); (iii) transition state (2.04–2.52 mW); (iv) pure hydrophobic state (>2.52 mW).

is induced by the light scattering. (iii) Transition state (2.04–2.52 mW): with irradiation light power further increased, the PNIPA exceeds the critical temperature. The phase transition is triggered, which results in the strong increase of the refractive index (wavelength redshift) and light scattering (linewidth broadening). Compared with the subtransition state, the wavelength shift and linewidth broadening in this stage are significantly enhanced by over 2 times and 8 times, respectively. (iv) Pure hydrophobic state (>2.52 mW): the phase-transition process of PNIPA is completed, as indicated by the nearly constant linewidth of the WGM. The wavelength redshift is only contributed to by the light absorption of water. Note that the wavelength shift is dominated by the temperature change in silica, where most of the mode energy is confined. The combination of wavelength shift and linewidth broadening provides the unambiguous evidence of the PNIPA phase-transition process.

Finally, to continuously measure the dynamic phase transition of PNIPA, the wavelength shift and linewidth broadening of the MBR are monitored in real time, as shown in Figs. 4(a) and 4(b), respectively. When the irradiation light is off, the resonance wavelength and linewidth are almost unchanged, as

expected. In contrast, the resonance wavelength experiences an overall redshift when the irradiation light power (3.00 mW at 1550 nm) is switched on at 12.5 s. The sharp increase of wavelength redshift in the beginning is mainly induced by the sudden temperature rise of the MBR, which is contributed to by the PNIPA absorption and heat conduction. The increase in temperature triggers the phase transition of PNIPA. During the following hydrophilic to hydrophobic transition process, the wavelength shift is contributed to by the variations of the MBR temperature and refractive index. First, a small blueshift of 8.02 pm in wavelength is observed (13.22–15.62 s), since the PNIPA hydrophobic transition absorbs the heat from the environment [55], resulting in the temperature decrease of the MBR. Note that in this process, the contribution from the MBR temperature decrease dominates over that of the refractive index increase. Then a significant wavelength redshift (39.23 pm) is obtained due to the gradual increase of the MBR refractive index during the PNIPA hydrophobic transition process. Figure 4(b) shows the corresponding WGM linewidth change as the PNIPA undergoes a hydrophilic to hydrophobic transition. The linewidth is increased significantly from 0.38 to 4.34 GHz owing to the enhanced light scattering of the PNIPA
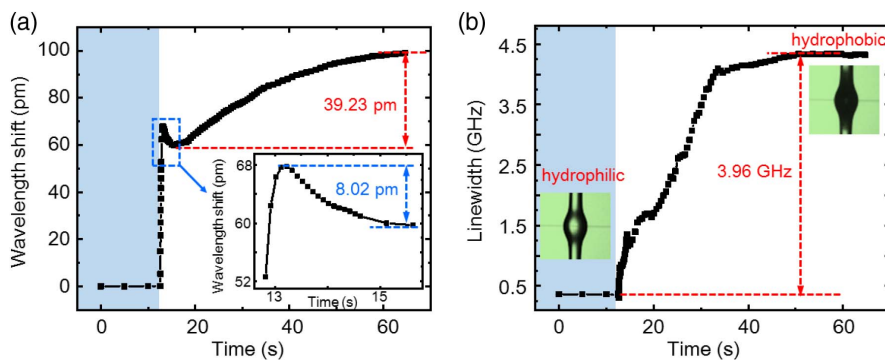

Fig. 4. (a) Real-time WGM resonance wavelength shift and (b) linewidth broadening during the PNIPA hydrogel phase transition (a hydrophilic to hydrophobic transition) monitored by an MBR. The control power of the irradiation light is switched on at ∼12.5 s. During the whole phase-transition process, a small blueshift of 8.02 pm in wavelength is first observed within 13.22–15.62 s; then the overall redshift of the resonance wavelength is 39.23 pm, and the maximized linewidth broadening is 3.96 GHz.

hydrophobic transition. Moreover, the optical responses of the MBR to the phase transition of PNIPA have been well reproduced in more than five devices.

4. CONCLUSION

In summary, we experimentally characterize the thermosensitive PNIPA hydrogel phase transition via an ultrahigh Q MBR sensor. By controlling the output power of the irradiation light, the optical tuning of the PNIPA hydrogel phase transition has been successfully achieved. Furthermore, we reveal the refractive index and temperature changes during the different stages of the phase transition process by monitoring the wavelength shift and linewidth broadening in real time. Our work demonstrates that MBR-based biosensors are promising for further quantitatively investigating the energy change during a phase transition, thus providing insights into their dynamic reaction mechanisms.

REFERENCES

1. A. Onuki, *Phase Transition Dynamics* (Cambridge University, 2002).
2. K. Kadau, T. C. Germann, P. S. Lomdahl, and B. Holian, "Microscopic view of structural phase transitions induced by shock waves," Science **296**, 1681–1684 (2002).
3. A. Cavalleri, C. Toth, C. W. Siders, J. A. Squier, F. Raksi, P. Forget, and J. C. Kieffer, "Femtosecond structural dynamics in VO₂ during an ultrafast solid-solid phase transition," Phys. Rev. Lett. **87**, 237401 (2001).
4. G. W. Ashley, J. Henise, R. Reid, and D. V. Santi, "Hydrogel drug delivery system with predictable and tunable drug release and degradation rates," Proc. Natl. Acad. Sci. USA **110**, 2318–2323 (2013).
5. S. P. Zustiak and J. B. Leach, "Characterization of protein release from hydrolytically degradable poly(ethylene glycol) hydrogels," Biotechnol. Bioeng. **108**, 197–206 (2011).
6. F. Ordikhani, S. P. Zustiak, and A. Simchi, "Surface modifications of titanium implants by multilayer bioactive coatings with drug delivery potential: antimicrobial, biological, and drug release studies," J. Miner. Met. Mater. Soc. **68**, 1100–1108 (2016).
7. M. Dompé, F. J. Cedano-Serrano, O. Heckert, N. van den Heuvel, J. van der Gucht, Y. Tran, D. Hourdet, C. Creton, and M. Kamperman, "Thermoresponsive complex coacervate-based underwater adhesive," Adv. Mater. **31**, 1808179 (2019).
8. A. M. Mathur and A. B. Scranton, "Characterization of hydrogels using nuclear magnetic resonance spectroscopy," Biomaterials **17**, 547–557 (1996).
9. K. M. Schultz, A. D. Baldwin, K. L. Kiick, and E. M. Furst, "Gelation of covalently cross-linked PEG-heparin hydrogels," Macromolecules **42**, 5310–5316 (2009).
10. K. J. Vahala, "Optical microcavities," Nature **424**, 839–846 (2003).
11. E. Betzig and R. J. Chichester, "Single molecules observed by near-field scanning optical microscopy," Science **262**, 1422–1425 (1993).
12. X. Fan, I. M. White, S. I. Shopova, H. Zhu, J. D. Suter, and Y. Sun, "Sensitive optical biosensors for unlabeled targets: a review," Anal. Chim. Acta. **620**, 8–26 (2008).
13. Y. Zhi, X.-C. Yu, Q. Gong, L. Yang, and Y.-F. Xiao, "Single nanoparticle detection using optical microcavities," Adv. Mater. **29**, 1604920 (2017).
14. H. Li, Y. Huang, G. Hou, A. Xiao, P. Chen, H. Liang, Y. Huang, X. Zhao, L. Liang, X. Feng, and B. Guan, "Single-molecule detection of biomarker and localized cellular photothermal therapy using an optical microfiber with nanointerface," Sci. Adv. **5**, eaax4659 (2019).
15. S. Frustaci and F. Vollmer, "Whispering-gallery mode (WGM) sensors: review of established and WGM-based techniques to study protein conformational dynamics," Curr. Opin. Chem. Biol. **51**, 66–73 (2019).
16. F. Vollmer and L. Yang, "Review label-free detection with high-Q microcavities: a review of biosensing mechanisms for integrated devices," Nanophotonics **1**, 267–291 (2012).
17. J. D. Swaim, J. Knittel, and W. P. Bowen, "Detection of nanoparticles with a frequency locked whispering gallery mode microresonator," Appl. Phys. Lett. **102**, 183106 (2013).
18. W. J. Chen, S. K. Ozdemir, G. M. Zhao, J. Wiersig, and L. Yang, "Exceptional points enhance sensing in an optical microcavity," Nature **548**, 192–196 (2017).
19. S. Q. Liu, B. J. Shi, Y. Wang, L. G. Cui, J. Yang, W. M. Sun, and H. Y. Li, "Whispering gallery modes in a liquid-filled hollow glass microsphere," Opt. Lett. **42**, 4659–4662 (2017).
20. J. Zhu, S. K. Ozdemir, Y.-F. Xiao, L. Li, L. He, D.-R. Chen, and L. Yang, "On-chip single nanoparticle detection and sizing by mode splitting in an ultrahigh-Q microresonator," Nat. Photonics **4**, 46–49 (2010).
21. T. Lu, H. Lee, T. Chen, S. Herchak, J.-H. Kim, S. E. Fraser, R. C. Flagan, and K. Vahala, "High sensitivity nanoparticle detection using optical microcavities," Proc. Natl. Acad. Sci. USA **108**, 5976–5979 (2011).
22. L. Shao, X. F. Jiang, X.-C. Yu, B.-B. Li, W. R. Clements, F. Vollmer, W. Wang, Y.-F. Xiao, and Q. Gong, "Detection of single nanoparticles and lentiviruses using microcavity resonance broadening," Adv. Mater. **25**, 5616–5620 (2013).
23. B.-B. Li, W. R. Clements, X.-C. Yu, K. Shi, Q. Gong, and Y.-F. Xiao, "Single nanoparticle detection using split-mode microcavity Raman lasers," Proc. Natl. Acad. Sci. USA **111**, 14657–14662 (2014).
24. S. K. Ozdemir, J. Zhu, X. Yang, B. Peng, H. Yilmaz, L. He, F. Monifi, S. H. Huang, G. L. Long, and L. Yang, "Highly sensitive detection of nanoparticles with a self-referenced and self-heterodyned whispering-gallery Raman microlaser," Proc. Natl. Acad. Sci. USA **111**, E3836–E3844 (2014).
25. K. D. Heylman, N. Thakkar, E. H. Horak, S. C. Quillin, C. Cherqui, K. A. Knapper, D. J. Masiello, and R. H. Goldsmith, "Optical microresonators as single-particle absorption spectrometers," Nat. Photonics **10**, 788–795 (2016).
26. J. Su, A. F. Goldberg, and B. M. Stoltz, "Label-free detection of single nanoparticles and biological molecules using microtoroid optical resonators," Light Sci. Appl. **5**, e16001 (2016).
27. X.-C. Yu, Y. Zhi, S.-J. Tang, B.-B. Li, Q. Gong, C.-W. Qiu, and Y.-F. Xiao, "Optically sizing single atmospheric particulates with a 10-nm resolution using a strong evanescent field," Light Sci. Appl. **7**, 18003 (2018).
28. X.-C. Yu, B.-B. Li, P. Wang, L. Tong, X.-F. Jiang, Y. Li, Q. Gong, and Y.-F. Xiao, "Single nanoparticle detection and sizing using a nanofiber pair in aqueous environment," Adv. Mater. **26**, 7462–7467 (2014).
29. N. Zhang, Z. Gu, S. Liu, Y. Wang, S. Wang, Z. Duan, W. Sun, Y.-F. Xiao, S. Xiao, and Q. Song, "Far-field single nanoparticle detection and sizing," Optica **4**, 1151–1156 (2017).
30. S.-J. Tang, S. Liu, X.-C. Yu, Q. Song, Q. Gong, and Y.-F. Xiao, "On-chip spiral waveguides for ultrasensitive and rapid detection of nanoscale objects," Adv. Mater. **30**, 1800262 (2018).
31. J. M. Ward, Y. Yang, F. Lei, X.-C. Yu, Y.-F. Xiao, and S. N. Chormaic, "Nanoparticle sensing beyond evanescent field interaction with a quasi-droplet microcavity," Optica **5**, 674–677 (2018).

32. H. Jing, H. Lü, S. K. Ozdemir, T. Carmon, and F. Nori, "Nanoparticle sensing with a spinning resonator," Optica **5**, 1424–1430 (2018).

33. M. R. Foreman, D. Keng, E. Treasurer, J. R. Lopez, and S. Arnold, "Whispering gallery mode single nanoparticle detection and sizing: the validity of the dipole approximation," Opt. Lett. **42**, 963–966 (2017).

34. F. Vollmer and S. Arnold, "Whispering-gallery-mode biosensing: label-free detection down to single molecules," Nat. Methods **5**, 591–596 (2008).

35. F. Vollmer, S. Arnold, and D. Keng, "Single virus detection from the reactive shift of a whispering-gallery mode," Proc. Natl. Acad. Sci. USA **105**, 20701–20704 (2008).

36. L. He, S. K. Ozdemir, J. Zhu, W. Kim, and L. Yang, "Detecting single viruses and nanoparticles using whispering gallery microlasers," Nat. Nanotechnol. **6**, 428–432 (2011).

37. I. Ament, J. Prasad, A. Henkel, S. Schmachtel, and C. Sonnichsen, "Single unlabeled protein detection on individual plasmonic nanoparticles," Nano Lett. **12**, 1092–1095 (2012).

38. V. R. Dantham, S. Holler, C. Barbre, D. Keng, V. Kolchenko, and S. Arnold, "Label-free detection of single protein using a nanoplasmonic-photonic hybrid microcavity," Nano Lett. **13**, 3347–3351 (2013).

39. M. D. Baaske, M. R. Foreman, and F. Vollmer, "Single-molecule nucleic acid interactions monitored on a label-free microcavity biosensor platform," Nat. Nanotechnol. **9**, 933–939 (2014).

40. J. Su, "Label-free single exosome detection using frequency-locked microtoroid optical resonators," ACS Photon. **2**, 1241–1245 (2015).

41. E. Kim, M. D. Baaske, and F. Vollmer, "In situ observation of single-molecule surface reactions from low to high affinities," Adv. Mater. **28**, 9941–9948 (2016).

42. W. Yu, W. C. Jiang, Q. Lin, and T. Lu, "Cavity optomechanical spring sensing of single molecules," Nat. Commun. **7**, 12311 (2016).

43. S. Subramanian, H.-Y. Wu, T. Constant, J. Xavier, and F. Vollmer, "Label-free optical single-molecule micro-and nanosensors," Adv. Mater. **30**, 1801246 (2018).

44. E. Kim, M. D. Baaske, I. Schuldes, P. S. Wilsch, and F. Vollmer, "Label-free optical detection of single enzyme-reactant reactions and associated conformational changes," Sci. Adv. **3**, e1603044 (2017).

45. Z. Li, C. Zhu, Z. Guo, B. Wang, X. Wu, and Y. Fei, "Highly sensitive label-free detection of small molecules with an optofluidic microbubble resonator," Micromachines **9**, 274 (2018).

46. Y. Zhang, T. Zhou, B. Han, A. Zhang, and Y. Zhao, "Optical biochemical sensors based on whispering gallery mode resonators," Nanoscale **10**, 13832–13856 (2018).

47. M. D. Baaske and F. Vollmer, "Optical observation of single atomic ions interacting with plasmonic nanorods in aqueous solution," Nat. Photonics **10**, 733–739 (2016).

48. S. H. Huang, S. Sheth, E. Jain, X. Jiang, S. P. Zustiak, and L. Yang, "Whispering gallery mode resonator sensor for in situ measurements of hydrogel gelation," Opt. Express **26**, 51–62 (2018).

49. H. G. Schild, "Poly(N-isopropylacrylamide): experiment, theory and application," Prog. Polym. Sci. **17**, 163–249 (1992).

50. B. Jeong, S. W. Kim, and Y. H. Bae, "Thermosensitive sol-gel reversible hydrogels," Adv. Drug Delivery Rev. **64**, 154–162 (2012).

51. M. Xiong, B. Gu, J.-D. Zhang, J.-J. Xu, H.-Y. Chen, and H. Zhong, "Glucose microfluidic biosensors based on reversible enzyme immobilization on photopatterned stimuli-responsive polymer," Biosens. Bioelectron. **50**, 229–234 (2013).

52. Y. Zhou, Y. Cai, X. Hu, and Y. Long, "Temperature-responsive hydrogel with ultra-large solar modulation and high luminous transmission for smart window applications," J. Mater. Chem. A **2**, 13550–13555 (2014).

53. Y. Ding, X. Ye, and G. Zhang, "Microcalorimetric investigation on aggregation and dissolution of poly(N-isopropylacrylamide) chains in water," Macromolecules **38**, 904–908 (2005).

54. H. Cheng, L. Shen, and C. Wu, "LLS and FTIR studies on the hysteresis in association and dissociation of poly(N-isopropylacrylamide) chains in water," Macromolecules **39**, 2325–2329 (2006).

55. G. Graziano, "On the temperature-induced coil to globule transition of poly-N-isopropylacrylamide in dilute aqueous solutions," Int. J. Biol. Macromol. **27**, 89–97 (2000).

56. A. Burmistrova, M. Richter, M. Eisele, C. Üzüm, and R. Von Klitzing, "The effect of co-monomer content on the swelling/shrinking and mechanical behaviour of individually adsorbed PNIPAM microgel particles," Polymers **3**, 1575–1590 (2011).

57. S. Cai and Z. Suo, "Mechanics and chemical thermodynamics of phase transition in temperature-sensitive hydrogels," J. Mech. Phys. Solids **59**, 2259–2278 (2011).